Molecular Mechanisms of Sorbed Ion Effects During Boehmite Particle Aggregation

Tingting Liu[1], Nikhil Rampal[1], Elias Nakouzi[2], Benjamin A. Legg[2], Jaehun Chun[2], Lili Liu[2], Gregory K. Schenter[2], James J. De Yoreo[2], Lawrence M. Anovitz[1], and Andrew G. Stack[1*]

[1]*Chemical Sciences Division, Oak Ridge National Laboratory, Oak Ridge, Tennessee 37831, United States*
[2]*Physical and Computational Sciences Directorate, Pacific Northwest National Laboratory, Richland, Washington 99354, United States*

**Corresponding author: stackag@ornl.gov*

Notice: This manuscript has been authored by UT-Battelle, LLC, under contract DE-AC05-00OR22725 with the US Department of Energy (DOE). The US government retains and the publisher, by accepting the article for publication, acknowledges that the US government retains a nonexclusive, paid-up, irrevocable, worldwide license to publish or reproduce the published form of this manuscript, or allow others to do so, for US government purposes. DOE will provide public access to these results of federally sponsored research in accordance with the DOE Public Access Plan (http://energy.gov/downloads/doe-public-access-plan).

Abstract

Classical theories of particle aggregation, such as Derjaguin-Landau-Verwey-Overbeek (DLVO), do not explain recent observations of ion-specific effects or the complex concentration dependence for aggregation. Thus, here, we probe the molecular mechanisms by which selected alkali nitrate ions (Na^+, K^+, NO_3^-) influence aggregation of the mineral boehmite (γ-AlOOH) nanoparticles. Nanoparticle aggregation was simulated using classical molecular dynamics (CMD) simulations coupled with the metadynamics rare event approach for stoichiometric surface terminations of two boehmite crystal faces. Calculated free energy landscapes reveal how electrolyte ions alter aggregation on different crystal faces relative to pure water. Consistent with experimental observations, we find that adding an electrolyte significantly reduces the energy barrier for particle aggregation (~3-4×). However, in this work we show this is due to the ions disrupting interstitial water networks, and that aggregation between (010) basal–basal surfaces is more favorable than between (001) edge–edge surfaces (~5-6×) due to the higher interfacial water densities on edge surfaces. The interfacial distances in the interlayer between aggregated particles with electrolytes (~5-10 Å) is larger than those in pure water (a few Ångströms). Together, aggregation/disaggregation in salt solutions is predicted to be more reversible due to these lower energy barriers, but there is uncertainty on the magnitudes of the energies that lead to aggregation at the molecular scale. By analyzing the peak water densities of the first monolayer of interstitial water as a proxy for solvent ordering, we find that the extent of solvent ordering likely determines the structures of aggregated states as well as the energy barriers to move between them. The results suggest a path for developing a molecular-level basis to predict the synergies between ions and crystal faces that facilitate aggregation under given solution conditions. Such fundamental understanding could extensively be applied to the aggregation and precipitation utilization in the

68 biological, pharmaceutical, materials design, environmental remediation, and geological regimes.

69 **Key words:** boehmite; nanoparticle; aggregation; classical molecular dynamics; metadynamics;
70 hydrogen bonding; free energy surface; energy barrier; DLVO; electrolyte

71 # 1. Introduction

72 Particle aggregation is a widespread phenomenon in natural environments and in various
73 industrial, biomedical and environmental remediation settings.[1,2] Aggregation is affected by many
74 factors, including solution chemistry (pH, electrolyte composition and concentration) and particle
75 morphologies (specific crystal faces and shape), creating a complex interplay that sometimes
76 defies[3–5] classical descriptions of aggregation based solely on electrostatic repulsion due to surface
77 charge and van der Waals interactions (e.g., the Derjaguin-Landau-Verwey-Overbeek, or DLVO,
78 theory).[6,7] Short-range forces such as those from hydration are poorly understood in particular.[8,9]
79 For example, using the surface force apparatus (SFA), Israelachvili and Pashley interpreted four
80 ordered layers of interfacial water between two mica surfaces within 1 nm.[10] However, it is not
81 clear whether the measured peaks in forces are due to the solvation structure itself[10] or perhaps
82 arise from electrolyte ion correlation and/or ordering.[9,11] To improve upon inconsistencies between
83 observed behaviors, especially ion specific effects, the mechanisms of aggregation, specifically a
84 correlation between interfacial structures and corresponding forces at the molecular level must be
85 understood.

86 A recently developed method to obtain molecular-level structure and dynamics during
87 aggregation combines classical molecular dynamics (MD) simulations with rare event methods
88 that bias the simulation to obtain information about processes that are too slow to observe directly.
89 Specific studies using this method include analysis of the minerals montmorillonite
90 ($(Na,Ca)_{0.33}(Al_{3.2}Mg_{0.8})Si_8O_{20}(OH)_4 \cdot nH_2O$)[4,5] in water and electrolyte solutions and gibbsite (γ-

$Al(OH)_3$)[12,13] in pure water. These show that most common states for attachment involve one or two monolayers of water between the nanoparticles. Ho et al.[12,13] used umbrella sampling to examine gibbsite nanoplatelet aggregation in different orientations, i.e., basal–basal, edge–edge, and basal–edge, as well as the rotating and sliding motions between two platelets.[13] They found that removing the last layer of water between two platelets required overcoming an energy barrier of hundreds of kJ/mol. The activation energy for this process is sufficiently large that it is unlikely to occur at a significant level at room temperature. This finding, of large barriers to fully dehydrate particles during aggregation, is consistent with an experimental TEM study[14] on fibrous boehmite composed of ~1 nm wide strips ~6.8 Å thick (which may include oriented aggregation during nucleation). Regarding the structure of solutions at interfaces, Nakouzi et al. explored the water-boehmite interface structure using 3D fast force mapping (FFM) coupled with MD simulations.[15] They found four ordered water layers within 1 nm on the surface.

Here, we explore the origins of the effects of electrolyte species on the aggregation mechanisms of boehmite (γ-AlOOH) nanoparticles to understand the likely behavior of this material in legacy wastes during storage and processing. At the Hanford site in Washington state, U.S.A., high pH and high salinity radioactive materials are dominated by aluminate anions ($Al(OH)_4^-$), the aluminum (oxy)hydroxide solid phases gibbsite and boehmite,[16–18] and cation solute species is dominated by Na^+.[16,19] The variable compositions of these slurries and their propensity to aggregate makes developing strategies for waste processing challenging.[20,21] Aggregates exist within the tanks,[22] and unexpected aggregation can occur in processing lines. Thus, a molecularly-informed understanding of aggregation will be uniquely beneficial to develop methods to process these materials and furthermore, provide a understanding of how salt solutions promote aggregation in various natural and industrial settings such as crystal growth and

wastewater treatment.

What is known about aggregation in this system is derived from a recent study of boehmite particle aggregation in alkali nitrate solutions at different concentrations that quantified aggregation as a function of electrolyte species and concentration (up to 2 molal, to emulate high salinities in the waste tanks) using small angle neutron scattering (SANS) experiments.[3] Figure 1 shows the cumulative particle mass fraction up to 1 μm in MNO_3 solutions (M = H, Li, Na, K and Rb) as a function of concentration.[3] The total boehmite concentration was 20 mass % in each system and downward on the *y*-axis represents an increase in the fraction of aggregates larger than 1 μm, and thus the solid buffered the pH of the solution (except in HNO_3), which was in the range 8.8-9.0 at concentrations greater than 0.1 molal (*m*). While boehmite has shown a morphology-dependent point of zero charge (p.z.c.), in this study, the pHs of the solutions (except HNO_3) were buffered by the mineral surfaces themselves and were close to the pH p.z.c. found for boehmite platelets (~8.5-9.5).[23,24] Thus, it is safe to assume that the aggregation in this study was observed under conditions without significant amounts of net surface charge of the boehmite. Surface charge strongly affects aggregation propensity, with a large coulombic repulsion between surfaces inhibiting aggregation, but apparent charge reversals due to sorbed species and ion pair formation can confound interpretation.[25]

Regardless, in the Anovitz et al. (2022) study, at low concentrations (10^{-5} *m*, 10^{-3} *m*, and 0.1 *m*), increasing the electrolyte concentrations facilitates an increase in aggregation (in contrast to nitric acid). However, this trend reverses at a critical concentration (e.g., 0.1 *m* for $NaNO_3$), beyond which increasing the electrolyte concentration (0.3 *m*, and 2 *m*) leads to decreased aggregation. Except for sodium, the larger the alkali cation, the more it promotes aggregation. Sodium was found to facilitate aggregation to a greater extent than other alkali cations. Simulations

of the (010) surface found a stronger adsorption affinity for Na^+ than K^+ to the basal surface.[3] That is, Na^+ ions have a greater propensity to form inner-sphere adsorbed species than the larger K^+, which lie in outer-sphere positions. This suggests Na^+ ions promote particle aggregation more efficiently than other alkali cations because they can fit in a site on the particle surface, helping to neutralize surface change. Here we test the hypothesis generated from this prior work, that the different hydration size and free energy of monovalent cations can drive different effects and mechanisms during particle aggregation by comparing Na^+ with the larger K^+, without confounding columbic effects induced by variable surface charges. Beyond this specific system, it is known that divalent (and trivalent) cations tend to adsorb more strongly to mineral surfaces when the surfaces have a negative charge[26] and have a subsequent influence on aggregation extent.[27–29]

Beyond salt effects, in this system particle aggregation can also be enhanced by oriented attachment (OA).[30] This has been observed in real-time, liquid-cell TEM experiments,[31] wherein two particles align their crystallographic axes prior to colliding and fusing into a larger particle. For example, Figure 1b shows preferential aggregation of boehmite particles on the (010) basal surfaces in $NaNO_3$(aq). In addition to the observed OA between boehmite nanoparticles, Nakouzi et al. quantified the structure and the collective dynamics of the aggregates as a function of particle morphology and solution chemistry.[32] It is clear that the crystal-face specific dependent surface charge mentioned above[24] drives the differing aggregation behaviors as a function of pH. For boehmite platelets, such as those studied in Anovitz et al. (2022),[3] pHs near the p.z.c. (8.5-9.5) favor aggregation by basal (010) surfaces sites because the edge sites have significant positive surface charge and basal surfaces have zero charge. Higher pHs favor aggregation by edge sites (e.g., (101), (100), (001)), because these are uncharged under alkaline conditions, whereas the

basal surfaces develop a negative charge.[24,33] Despite this ongoing research, the energetics and detailed interfacial structure for particle aggregation in the absence/presence of electrolytes is still a principle knowledge gap from this system.

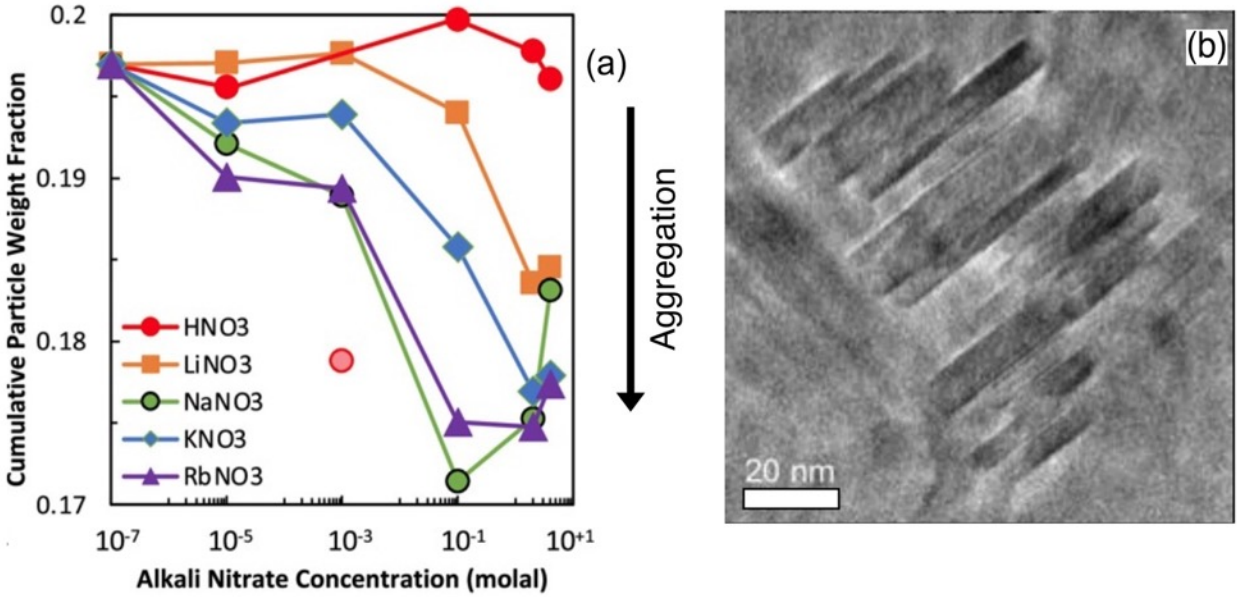

Figure 1. Previous experimental observation for boehmite particle aggregation. (a) Results from SANS data. The cumulative mass fraction of particles is 1 μm and smaller as a function of electrolyte composition and concentration. Reproduced from Anovitz et al.[3] Copyright 2022 American Chemical Society. (b) Cryo-TEM image of an aggregated boehmite in 0.01 M $NaNO_3$ solution (measured pH of 9). The stacking indicates a (010) basal–basal orientation is preferred. Reproduced from Anovitz et al.[31] Copyright 2018 American Chemical Society.

While the effects of electrolyte ions on aggregation are well documented, the theoretical underpinning of this effect is less clearly known. DLVO[6,7] theory predicts that an electrolyte promotes aggregation because counterions shield surface charge and decreases diffuse the layer thickness. As stated above, in the Anovitz et al. (2022) study (Figure 1a),[3] except for nitric acid, the solid surface was the dominant buffer of solution pH (in the range of 9.2[34] – 11.6[35] for boehmite, whereas Anovitz et al.[3] found pH 8-9). Thus, the basal surfaces should have little net surface charge, whereas the edge sites will have a positive charge. Since aggregation occurs by the basal surfaces under these conditions (Figure 1b), it is therefore, unclear why sorbed ions would

promote aggregation. DLVO[6,7] is based on continuum descriptions for particle interactions and cannot explain the observations. The main non-DLVO forces for inorganic nanoparticles in electrolyte solutions, i.e., the short-range repulsive hydration force during aggregation, have been validated in force measurements,[36–42] but the detailed interfacial structure in this short range (< ~1 nm) needs to rely on simulations.[4] To gain molecular-level understanding of aggregation in this system, we have used simulations to probe attachment of two nanoparticles through basal–basal aggregation, and used edge–edge aggregation as a contrast, in pure water or sodium and potassium nitrates sorbed in the interlayer between aggregating boehmite particles. This study shows the discrete interfacial solvent-solute distributions, as well as the roles that solvent and solute species play in driving aggregation. The energy landscape presented in this study helps us to elucidate the energetics and corresponding structural information for each aggregated state. Our study fills the knowledge gap about a correlation between short-range forces and the roles of solvent and solutes in promoting/inhibiting aggregation that elude classical aggregation theory.

2. Methods

Classical Molecular Dynamics (CMD) simulations were performed using empirical force fields and the LAMMPS software package.[43] All simulations were conducted at 300 K using the NVT ensemble with a time step of 1 fs. Periodic boundary conditions were applied in all directions. A cutoff distance of 10 Å was used and long-range Coulombic energy was estimated using the particle-particle particle-mesh (pppm) method[44] with a precision of 5×10^{-5}. The CLAYFF force field[45,46] was used for boehmite, which has been a focus for the model development.[47–49] Improved descriptions for the M-O-H angle on the edge[48,49] and the O-H bond[47] in the crystal structure were applied. Additional angle terms with large empirical constant values must be applied for edge atoms to stabilize solvated systems, particularly for biased simulations. Ho et al.[12] reported the

same approach that examined the aggregation behavior of solvated gibbsite particles. The SPC/E model for water[50] was used in this study.

To model basal–basal and edge–edge aggregation, two simulation box sizes were created: 100 Å × 100 Å × 100 Å, and 100 Å × 60 Å × 150 Å, to facilitate the analysis of basal–basal and edge–edge geometries, respectively. Two boehmite (*Cmcm* space group, a = 2.876 Å, b= 12.24 Å, c = 3.709 Å[51]) nanoparticles were placed in each simulation box. Each consisted of 15 × 2 × 15 unit cells (7440 atoms each) surrounded by an additional 90,000 water molecules, ensuring an appropriate bulk-like density for water at ambient conditions. Figure 2 shows the positions of the two nanoparticles oriented along the [010] for basal–basal attachment, and along the [001] for edge–edge attachment. For simplicity and to provide a direct contrast, uncharged, stoichiometric terminations of the surfaces were used, but in a real system, crystal-face specific surface charge would lead to at least one surface on platelets (basal or non-basal) to have significant charge. Our choice of uncharged surfaces is justified in that the goal of the study is to determine how short-range forces drive aggregation, and the data of Anovitz et al. (2022)[3] that we are working to explain, was performed under pHs where the basal (010) surfaces were uncharged. The edge sites are similarly chosen to be uncharged in order to determine how the structure of the mineral-water interface affects aggregation in a direct comparison. Adding a surface charge would add additional electrostatic repulsion to the system which would confound the interpretation.

All the atoms in the system were allowed to move, except for a block of atoms on the side of one of the nanoparticles opposite to where aggregation occurs. These were frozen to provide an absolute reference frame while biasing the other nanoparticle and to minimize rotational or translational motions. Before selecting force fields for $NaNO_3$ and KNO_3, literature sources were screened to obtain approximate values for the ion hydration energies (ΔH_{hyd}). These were

subsequently compared with experimental values (Table S1 in the Supporting Information).[52] The values of Fantauzzo et al.[53] were selected for Na^+, which are force fields for the solid-aqueous phase of alkali nitrates. The K^+ force field is from Wang et al.,[54] who developed them for a concentrated KNO_3 aqueous solution using neutron pair distribution function (PDF) analysis coupled with classical MD simulations. For NO_3^-, the interatomic potentials, bond, and angle constants are from Refs[55–57]. A summary of the interatomic potentials along with the bond and angle terms used in this study is given in Table S2 in the Supporting Information.

As discussed above, $NaNO_3$ generates maximum particle aggregation at a concentration of ~0.1 m, but at higher concentrations (to 2 m), this trend is reversed.[3] Unfortunately, we do not know the precise adsorption density of sodium or nitrate on boehmite (nor any other alkali nitrate salt) at these ionic strengths, much less crystal-face specific adsorption densities. While experimental adsorption isotherms are unavailable, we can estimate the adsorption isotherms from previous metadynamics results:[3] the equilibrium constants (K_{eq}) for ion adsorption on charge-neutral surface are 1120 and 36 for Na^+ and K^+, respectively, using the method described in Stack and Rustad,[58] and Rampal et al.[59] From the simulated thermodynamics of adsorption, we estimate that essentially all the cations would adsorb on the two boehmite surfaces under this simulation cell size at a bulk solution concentration of ~0.3 m (see the estimation using K_{eq} in the Sec I in the Supporting Information). This is a limitation of the finite simulation cell size relative to the experiments. Thus, to probe the effects of the electrolyte on aggregation most efficiently, we pre-adsorbed ions onto interstitial boehmite surfaces in these simulations. Thus, given the uncertainties in the equilibrium constants for adsorption derived from the CMD force fields, the results should be viewed as a general guide to the effects of adsorbed electrolyte ions not as corresponding to a specific concentration. A pure water scenario was also examined.

Figure 2 shows the aggregation topologies in pure water (Figures 2a, 2b) and with pre-sorbed sodium and nitrate ions (Figures 2c, 2d). Water molecules and ions were populated using Packmol.[60] While a more dilute system with a random distribution of ions was also examined (Figure S1 in the Supporting Information), ion effects were not observed due to the low ion density in the interlayer. Thus, the following results are only based on the pre-adsorbed ion scenario.

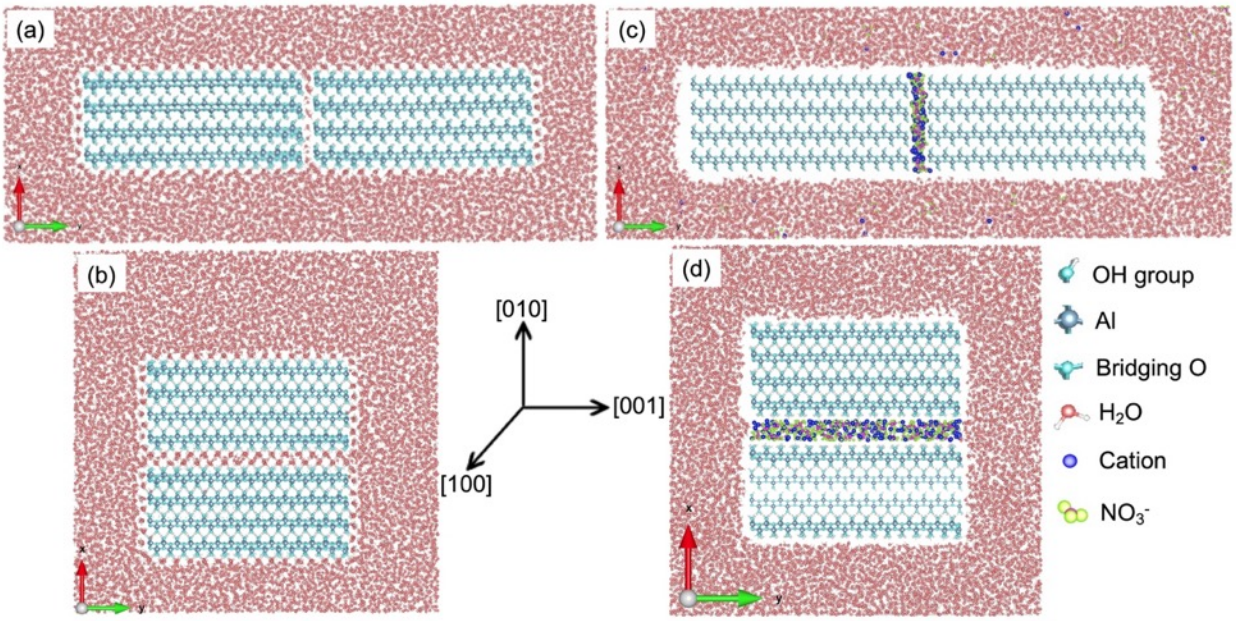

Figure 2. Side views of the simulation boxes. (a) and (b) show the particles in pure water in edge–edge and basal–basal configurations, respectively. (c) and (d) show the particles interfaced with a high ion concentration in edge–edge and basal–basal alignments, respectively. The view of the supercells has been truncated along the [100] direction to show the nanoparticles more closely.

Rare event simulations were performed with well-tempered metadynamics using the PLUMED[61–63] plugin for LAMMPS. Multiple walkers[64] were employed for efficient sampling, and the results were combined and processed by PLUMED[61–63] to generate the (Helmholtz) free energy surface or landscape (ΔF*). A reductionist collective variable (CV) was used to provide quantitative insights and facilitate observation and interpretation. Specifically, the center-of-mass (COM) distance between the two slabs was used here, but particles in real systems can exhibit far more complicated dynamics. To minimize translational and rotational motions during simulation,

first, the velocity of the center of mass of one of the particles was set to zero by freezing a block of its atoms. Then, only movement along the CV direction was allowed for the second particle, i.e., particle velocities in the *x* and *y* directions were set to zero (where the CV is along the *z* direction). An upper limit bias in the form of a repulsive wall was applied to the interfacial distance (COM minus one slab thickness) at ~ 15 Å for both basal–basal and edge–edge aggregation to avoid exploration of diffusional motions that do not contain significant energy barriers. No lower limit was used in order to maximize the chances of observing the complete collapse of the two particles where all interstitial water is expelled. The first step in the simulation process was to let the water and ions relax for 10 ps without relaxing the boehmite atoms. Next, the entire system was allowed to equilibrate for 0.5 ns before adding bias potentials to the system. Biasing was achieved by adding Gaussian-shaped repulsive potentials along the CV every 500 timesteps, with a height of 10 k_BT, a width of 0.1 Å, and a bias factor of 20. The latter was established by trial and error as an optimum value that allowed efficient exploration of the free energy surface. The two nanoparticles were set at different starting interfacial distances in each walker to further promote efficient exploration of the free energy surface. In the analysis of the results, we refer to local minima, which are interpreted as stable states, and to "barrier heights" between stable states, which form the local maxima. This term is used instead of the more usual "transition state" for the maxima in the free energy surfaces because the barriers observed do not necessarily correspond to individual bond breakages or formations.

3. Results & Discussion

3.1 Aggregation in Pure Water and with Adsorbed Ions

Figure 3 shows the free energy surfaces for aggregation by basal–basal and edge–edge interaction in pure water and with pre-adsorbed KNO_3 and $NaNO_3$ in the interlayer. The free

290 energy values have been normalized with respect to the interstitial surface areas of the basal or
291 edge surfaces of both particles, which makes it comparable between basal–basal and edge–edge
292 scenarios. The interstitial surface areas are $2 \times 43.14 \times 55.635$ Å^2, and $2 \times 43.14 \times 24.48$ Å^2 for
293 the basal and edge surfaces, respectively, including two contact surfaces. In addition, the energy
294 values were shifted so that the distance with the smallest amount of interaction between the
295 particles is at zero energy, close to the maximum distance. (These varied somewhat, likely at least
296 partially due to the repulsive potential used to enforce the boundary condition). The shifting was
297 performed by subtracting the almost unchanged energy value at the maximum distance from the
298 original calculated free energies that were processed by PLUMED.[61–63] The first notable feature
299 of these free energy surfaces is the large repulsive energy present at the smallest distances on every
300 data set. This is the barrier to dehydrate the interlayer entirely. The lack of resolved barriers (i.e.,
301 a peak, with minima on either side) indicates that the system never found a state in which the
302 interlayer had fully collapsed to a state without any interstitial water or salt species. Attempts to
303 force simulations to focus on the smaller distances and drive the system to complete dehydration
304 of the interlayer never fully sampled the energy barrier itself. When a simulation did achieve a
305 fully collapsed state, the dehydration was found to be irreversible because of hysteresis in the
306 interstitial water density. In the pure water case, some local minima (e.g., ~1.5 Å in Figure 3a) did
307 suggest the nanoparticles could be fully dehydrated by a "zipping" mechanism in which collapse
308 is initiated on one side of the particles and proceeds to the other (shown in Figure S3 in the
309 Supporting Information). While imperfect, these results indicate a significantly larger energy
310 barrier for complete dehydration than observed at higher hydration states, consistent with previous
311 work on gibbsite.[12,13]

312 For aggregation in pure water with some hydration of the interlayer, there are several,

relatively large, energy barriers at various states for both aggregation by basal–basal and edge–edge crystal surfaces (Figures 3a, b). The free energy minima for these states correspond to distances where stable networks of interstitial water form between the particles (Figures 4a, b). As the particles aggregate, each successive minimum corresponds to the removal of an additional water layer, as revealed by plots of the density of water as a function of interlayer distance (5 monolayers of water with a thickness of 11.5 Å down to 1 monolayer with a thickness of 2.5 Å for basal–basal aggregation). Barrier heights between stable hydration states are variable. The largest is from two monolayers of water (~5 Å) to one (~2.5 Å) for both basal–basal and edge–edge aggregations (Figures 4a, b), but the free energy barriers for basal–basal aggregation are dramatically lower than those for edge–edge aggregation, indicating a significant preference for basal–basal aggregation in pure water.

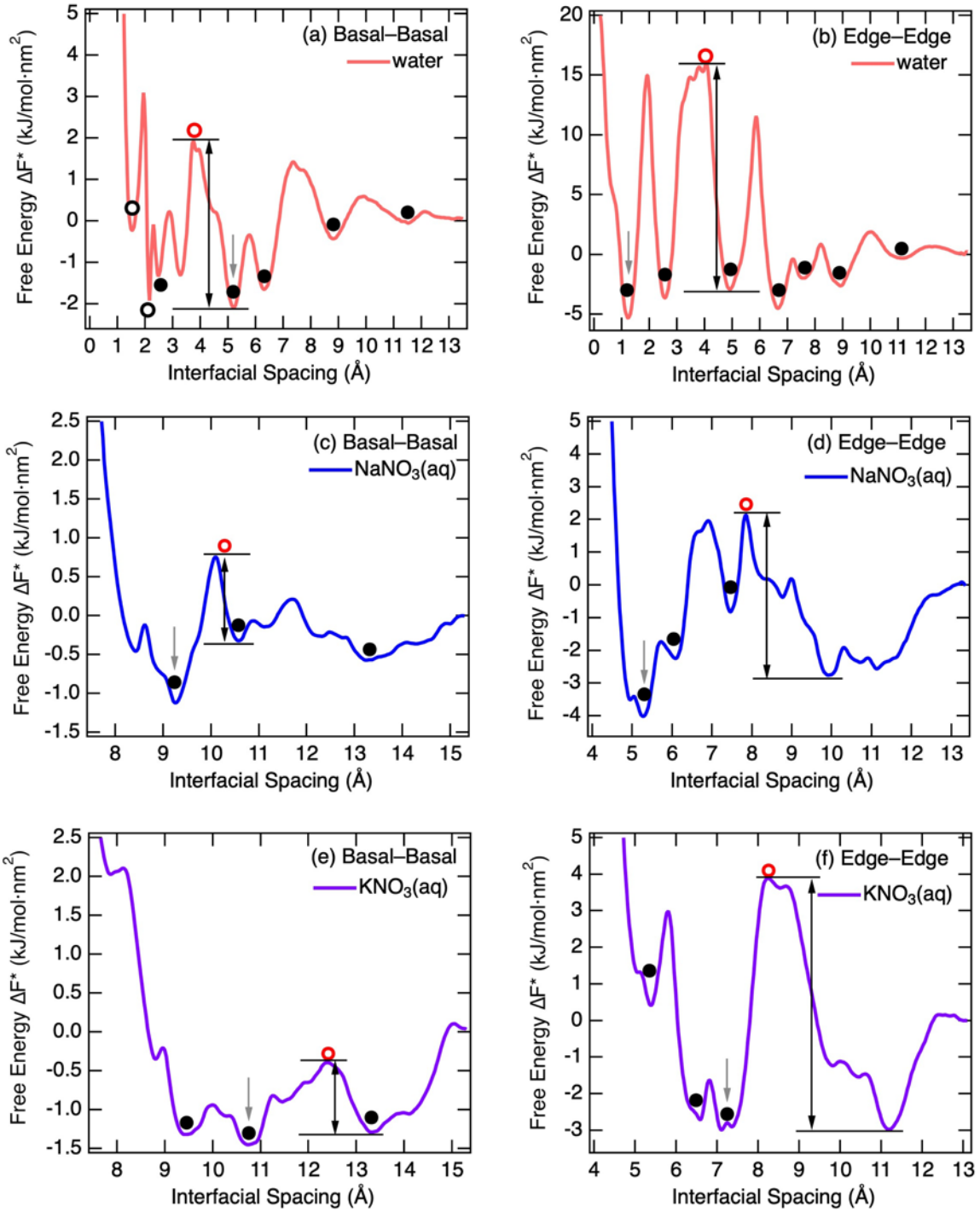

Figure 3. Free energy surface results for basal–basal aggregation: (a) in pure water, (c) with pre-adsorbed $NaNO_3$, (e) with pre-adsorbed KNO_3, and edge–edge aggregation: (b) in pure water, (d) with pre-adsorbed $NaNO_3$, and (f) with pre-adsorbed KNO_3. Filled black dots indicate the local minima and hollow black circles indicate partially collapsed nanoparticles. The red circles indicate the largest energy barriers to aggregation. The double-ended arrows indicate barrier heights, and the grey arrows indicate the global minima where aggregation is stabilized.

For a given aggregation orientation, the free energies for aggregation with pre-adsorbed ions are significantly smaller in magnitude, and the distances at which the energy minima are located are significantly larger, than in pure water. When solvated ions reside in the interlayer, they inhibit complete collapse of the interlayer. Table 1 summarizes the energy barriers estimated in this study (Figure 3) and compares the favorability of aggregation in the different media for the two orientations. The energy barriers are highly variable (Figure 3), but a measure of the relative favorability of aggregation is the magnitude of the largest energy difference between a stable minimum and the next maximum the particles experience as they approach each other during aggregation. These "limiting" barrier heights are highlighted in Figure 3, as are the lowest energy minima (global minima), which indicate the most stable state in which the aggregation will most commonly be found in a suspension.

The most notable conclusion that can be drawn from the free energy surfaces (Figure 3) is that the presence of pre-adsorbed electrolyte species lowers the energy penalty for basal–basal aggregation by a factor of ~3 to 4 relative to pure water (Table 1). This is consistent with the observation that aggregation is promoted in moderate ionic strength aqueous fluids relative to pure water (Figure 1).[3,31] This applies not just to the largest limiting barrier, but to the smaller energy barriers as well. Thus, aggregation should preferentially occur by basal–basal interaction, which is consistent with liquid-cell TEM results.[3,31] In fact, the barrier heights for edge–edge interaction are sufficiently high that it is difficult to understand how thermal motions (i.e., kT at room temperature, 2.5 kJ/mol) could produce such aggregation. However, our results showed no reduction in the barrier height for $NaNO_3$ relative to KNO_3. Since the experimental observations do show that $NaNO_3$ promotes aggregation more fully than KNO_3, this suggests that the ion sorption density itself is important for determining how efficiently ions promote aggregation. That

is, $NaNO_3$ may promote aggregation not because of the sodium ions themselves, but because more sodium adsorbs at a higher density than potassium (and perhaps nitrate through a synergistic effect by ion pair sorption). Our simulations, conducted at identical interstitial sorbed ion densities, would not be able to isolate this effect.

Table 1. Estimated maximum energy barriers to aggregation for each system in this study.

	Barrier Height (kJ/mol·nm^2)		Global minima, distance (kJ/mol·nm^2, Å)	
	Basal–basal	Edge–edge	Basal–basal	Edge–edge
water	4.0	18.8	-2.1, 5.2	-5.3, 1.2
$NaNO_3$(aq)	1.1	4.9	-1.1, 9.2	-4.0, 5.3
KNO_3(aq)	0.9	6.9	-1.5, 10.8	-3.0, 7.1

The interfacial distances in Table 1 show several additional results: (1) at the global minimum the solvated interlayer is thicker for the basal–basal than edge-edge orientation due to the ease of water layer formation on the basal surface (5.2 vs 1.2 Å; 9.2 vs 5.3 Å; 10.8 vs 7.1 Å); (2) the interfacial distance between aggregates in the presence of $NaNO_3$ is shorter than in the presence of KNO_3 (see distances of the representative local minima, Figure 3c vs 3e; Figure 3d vs 3f) because we find the global minimum occurs at a lower hydration state (shorter interparticle distance) for $NaNO_3$, and (3) aggregation by basal–basal interaction tends to occur at larger interlayer distances, likely due to the stronger hydrogen bonding network in the basal-basal configurations; and (4) the larger interfacial distances by the existence of the salts can potentially make the aggregates easily disaggregate, i.e., a reversible aggregation/disaggregation processes. Note that a rigorous understanding on the aggregation/disaggregation needs a consideration of the dispersion interaction between boehmite particles that is a main attractive contribution on the energy landscape. While the dispersion interaction between macroscopic bodies is intrinsically missing in the simulations, the presence of electrolytes is known to reduce the dispersion force (via reduced Hamaker constant) as a first approximation.[65] Further considering the separation

dependence of the dispersion force (i.e., an inverse of square of interfacial spacing), the larger interfacial distances by the existence of the salts lead to appreciably weak dispersion interactions, manifesting that the reversible aggregation/disaggregation is likely to be a reasonable rationale.

The above results should not be over-interpreted. The absolute values of the maxima may be inaccurate due to incomplete convergence of the free energy surface (a risk with metadynamics, see Figure S2 for a convergence analysis). Moreover, particle aggregation is a complex process, and our collective variable is a simplification. For example, we have made no effort to bias the water or electrolyte ion densities in the interlayers to determine their role in driving aggregation. However, it is unlikely that such effects will change the qualitative conclusions of the study. An additional factor that will change the outcome, however, is the effects of crystal-face specific surface charge. This is discussed in detail in Section 3.2 below.

3.1.1 Basal–Basal

Figures 4a-4e show representative structures and water densities for basal–basal aggregation in pure water with water layer thicknesses from ~2.5 to ~11.5 Å. These were selected from structures at the minima in Figure 3a. Water intercalating into the interfacial region creates a sandwiched structure with ordered layers close to the solid surfaces and fewer ordered layers in between. As expected, at the smallest distance of ~2.5 Å (Figure 4a), each water molecule interacts with typically two surface sites on each slab, forming two O_h-H_w and two O_w-H_h bonds. As hydration levels and the number of water monolayers are increased, there is a subtle shift in the densities of the sorbed water layer closest to the interfaces. While the minima at ~2.5 Å shows a slightly lower density in this layer, the minima at ~11.5 Å has a slightly higher density, suggesting that confinement at ~2.5 Å might prohibit the water from achieving an optimal structure. In addition, the two nanoparticles translate relative to each other by half a surface unit cell (compare

405 the dashed boxes in Figure 4a versus 4b). This occurs because, when only a single water layer is
406 present between the nanoparticles, each water molecule interacts with both particles, necessitating
407 a shift in the particle position (Figure 4a).

408 The density of the water at the energy maximum at ~3.7 Å is lower than that at the local
409 minima (Figure 4f). This suggests that the barriers to aggregation in pure water reflect the energy
410 necessary to reorganize the interstitial water to a new conformation at a lower hydration state.
411 Structures at the energy maxima at ~5.8 Å and ~7.4 Å (Figure S4) are consistent with this
412 observation. Additionally, at ~5.8 Å (Figure S4), the top particle has rotated slightly relative to the
413 bottom. This indicates that water was expelled/intercalated from/into the interlayer during
414 aggregation/disaggregation. This is demonstrated in Figure S5, which compares the extent of
415 rotation between two local minima and maxima. Prior simulations of water intercalation into the
416 interlayer of Na-montmorillonite shows similar rotation of the particles at their free energy
417 maxima.[66] The energy maxima during particle aggregation thus appear to be caused by unfavorable
418 spacing between nanoparticles at which water cannot comfortably form a hydrogen-bonded
419 network. At the local minima, in contrast, water can readily form energetically stable close-packed
420 layers. Numerous simulations have been performed on water structures between two solid slabs
421 comprising a slit pore, but the merit of this result is the discovery of a particular energy–structure
422 relationship at the mineral-water-mineral interface.

423
424
425

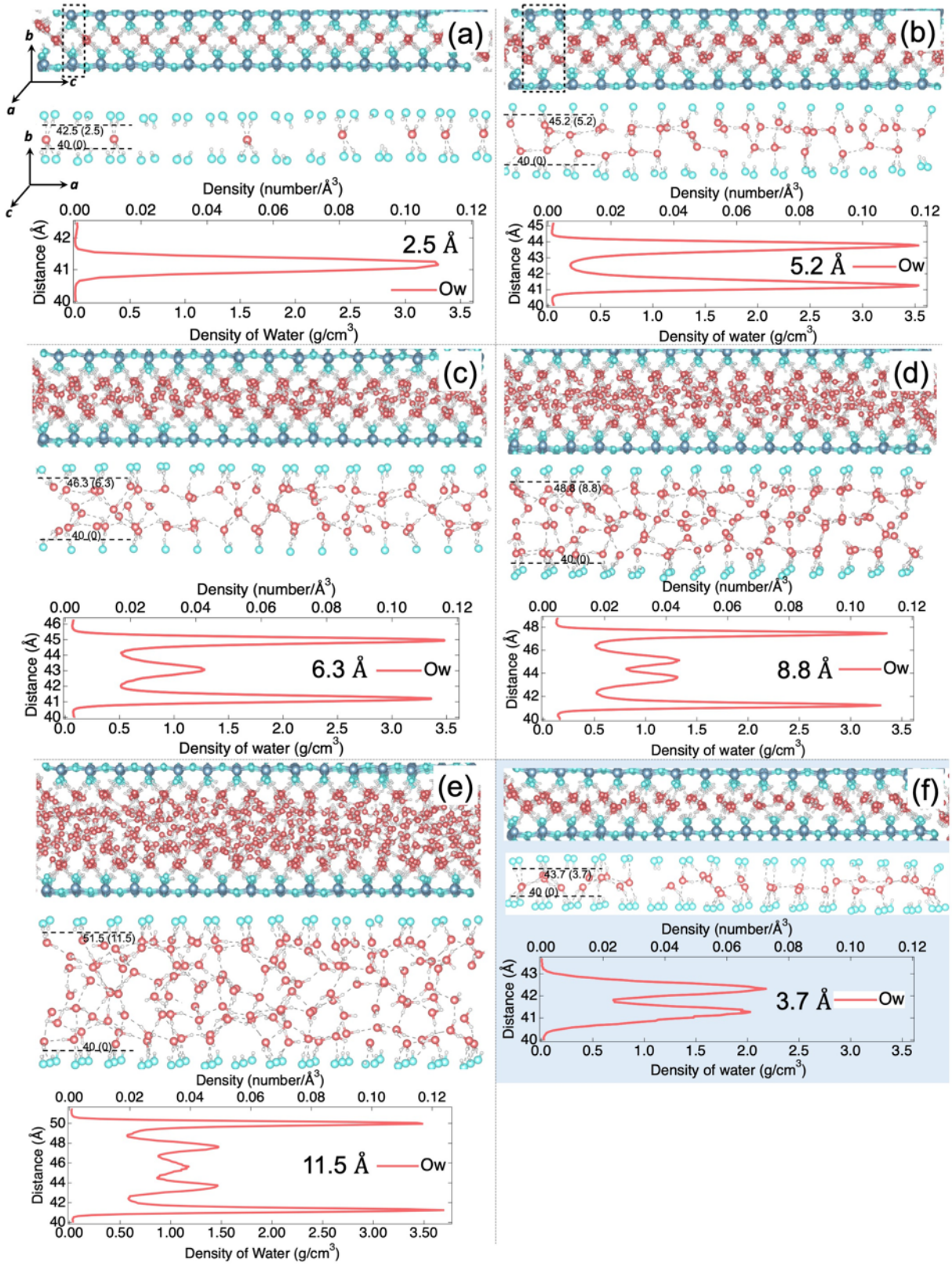

Figure 4. Local energy minima and one energy maximum (shown with a blue background) of boehmite particle basal–basal aggregation in pure water, with varying water layer thicknesses (a)

~2.5 Å, (b) ~5.2 Å, (c) ~6.3 Å, (d) ~8.8 Å, (e) ~11.5 Å, and (f) ~3.7 Å, chosen to correspond to the interfacial spacing denoted by the black dots and red circle in Figure 3a. The corresponding hydrogen bonding network and density profiles calculated using Ow atoms in the unit of number of atoms/Å^3 are shown below the snapshots. The interfacial configurations were rotated 90° and only certain rows were kept showing the hydrogen-bonding network. The dashed lines show the positions and distances between particles.

Figure 5 displays the structures, and solvent and ion densities of three local minima from both $NaNO_3$(aq) and KNO_3(aq) solution simulations (located at ~9.2, ~10.6, and ~13.3 Å), as well as one energy maximum configuration (~10.2 and ~12.4 Å for $NaNO_3$ and KNO_3, respectively). The local minima were selected at similar hydration states, but the energy maxima were selected globally. Overall, water densities are lower than that of pure water, which is to be expected as the concentration of ions in the interlayer is high. However, a qualitative inspection of the solvent structure suggests that the interlayer is also disordered relative to pure water: the networks of hydrogen-bonded water molecules found at low hydration levels are replaced by more complex and disordered structures involving water, cations, and nitrate. The aggregated state at a ~9.2 Å interparticle distance in electrolyte-containing solutions has four monolayers of water molecules. This is roughly the same distance at which four monolayers of water occur in pure water (~8.8 Å). All the water density profiles that illustrate the water with the interfacial electrolytes are summarized in Figures S6, S7 in the Supporting Information. At another higher hydration level, the comparison still holds between pure water (~11.5 Å, Figure 4e) and electrolyte-containing interfaces (~11.1 Å for $NaNO_3$, Figure S6; ~11.5 Å for KNO_3, Figure S7), all of which contain five layers of water. However, in both electrolyte-containing interfaces, the structure at the energy maximum is disordered relative to the minima, especially in the water molecule positions (Figures S6, S7). Overall, the solvent distribution and densities of the minima and maximum suggests that adsorbed ions reduce the barrier height to aggregation by allowing a more flexible hydrogen-bonding and ion-water network in the interlayer.

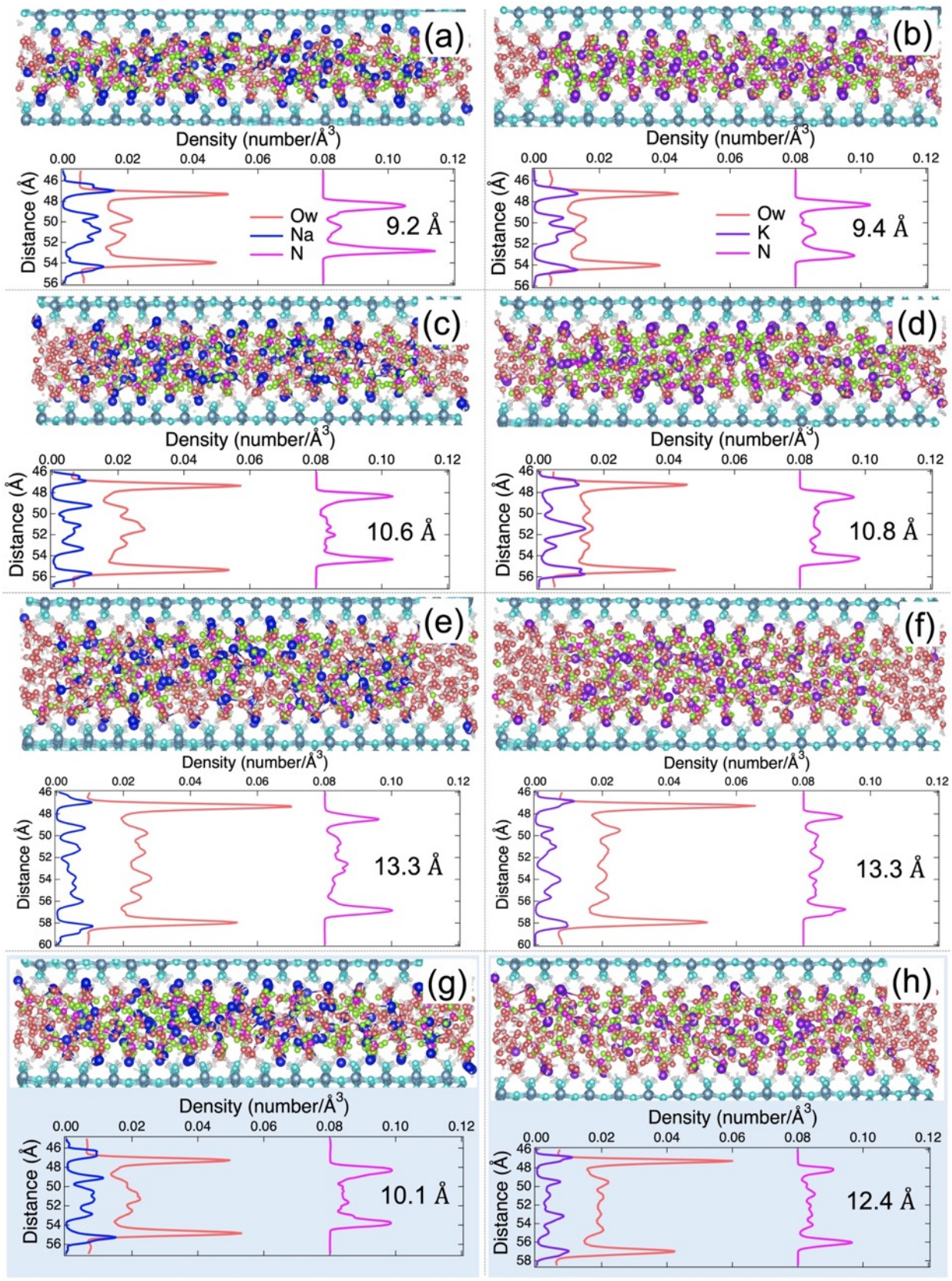
(a)
Density (number/Å^3)
0.00 0.02 0.04 0.06 0.08 0.10 0.12
Distance (Å)
46 48 50 52 54 56
Ow
Na
N
9.2 Å
(b)
Density (number/Å^3)
0.00 0.02 0.04 0.06 0.08 0.10 0.12
Distance (Å)
46 48 50 52 54 56
Ow
K
N
9.4 Å
(c)
Density (number/Å^3)
0.00 0.02 0.04 0.06 0.08 0.10 0.12
Distance (Å)
46 48 50 52 54 56
10.6 Å
(d)
Density (number/Å^3)
0.00 0.02 0.04 0.06 0.08 0.10 0.12
Distance (Å)
46 48 50 52 54 56
10.8 Å
(e)
Density (number/Å^3)
0.00 0.02 0.04 0.06 0.08 0.10 0.12
Distance (Å)
46 48 50 52 54 56 58 60
13.3 Å
(f)
Density (number/Å^3)
0.00 0.02 0.04 0.06 0.08 0.10 0.12
Distance (Å)
46 48 50 52 54 56 58 60
13.3 Å
(g)
Density (number/Å^3)
0.00 0.02 0.04 0.06 0.08 0.10 0.12
Distance (Å)
46 48 50 52 54 56
10.1 Å
(h)
Density (number/Å^3)
0.00 0.02 0.04 0.06 0.08 0.10 0.12
Distance (Å)
46 48 50 52 54 56 58
12.4 Å

456

Figure 5. Local minima and energy maxima of boehmite particle aggregation in $NaNO_3$(aq) and KNO_3(aq), showing density profiles for water, cations, and anions. The energy maxima are highlighted with a colored background. The left panel is for $NaNO_3$(aq) and the right for KNO_3(aq). The corresponding interfacial spacings for the local minima are ~9.2 Å (a), ~10.6 Å (c), and ~ 13.3 Å (e) for $NaNO_3$(aq); ~9.4 Å (b), ~10.8 Å (d), and ~ 13.3 Å (f) for KNO_3(aq). The energy maxima have the spacings of ~10.1 Å (g, $NaNO_3$) and ~12.4 Å (h, KNO_3), respectively. Lines between cations and Ow atoms in (a) – (h) indicate local hydration bonding between cations and water molecules. The density of NO_3^- is offset by 0.08 unit for clarity.

3.1.2 Edge–Edge

The structures of the seven local minima for edge-edge aggregation in pure water are shown in Figure 6. As with basal-basal interactions, nanoparticles rotate relative to each other during aggregation (see global views in Figure S8 in the Supporting Information), and likely form a hydrogen-bonded water network between surface sites and interstitial water. However, as noted above, the barrier heights for edge–edge aggregation are higher than those for basal–basal interactions. In addition, the interstitial water densities are greater for the edge–edge aggregates (> ~0.18 $H_2O/Å^3$) than for basal–basal aggregates (~0.10 $H_2O/Å^3$), suggesting that the energy barriers to disrupt those water structures might be correspondingly higher. The water densities can be explained by the differences in the interfacial structures and moieties on the edges and basal surfaces, which lead to different adsorption and hydration structures. That is, the edge surface of the (001) facet is terminated by η-water molecules (coordinating aluminums that would be otherwise unsaturated), μ_2- and μ_3-bridging oxygens, and η-hydroxyl groups; whereas the basal surface is only terminated with μ_2-hydroxyl groups and μ_4-bridging oxygens. Thus, there is a higher density of adsorption sites on the edges than on the basal surfaces. The adsorbed water densities are estimated to be 12 and 20 per nm^2 for basal–basal and edge–edge interactions, respectively, for aggregates where each surface has a full monolayer of water on it (2 ML of interstitial water total). This means that reorganizing to a new configuration requires more bonds to be broken and reformed in the edge–edge orientation and a correspondingly higher barrier

height.

However, at larger distances (Figures 6e–6g), the middle layers are less well-ordered with increasingly lower peak densities, even lower than those in the basal–basal interactions. This less strong hydrogen bonding network could account for why the energy barriers are lowered at these more hydrated states (Figure 3b). Although such aggregates are easy to achieve, they also may not be as stable due to the less strong hydrogen bonding network.

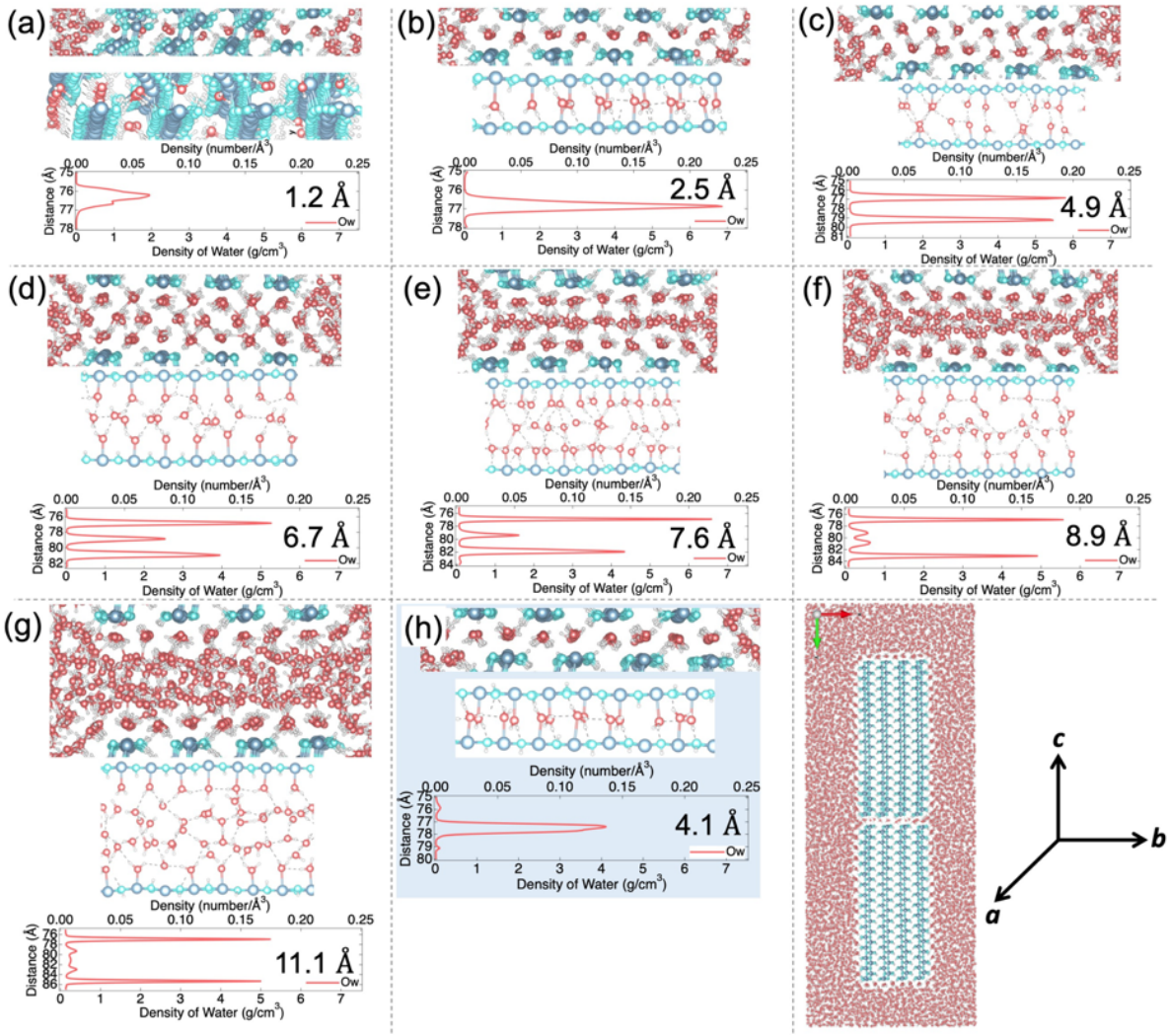

Figure 6. Local minima for boehmite particle edge–edge aggregation in pure water. (a) – (g) show ~1.2 Å, ~2.5 Å, ~4.9 Å, ~6.7 Å, ~7.6 Å, ~8.9 Å, and ~11.1 Å interfacial spacings, respectively. Energy maxima occur at ~4.1 Å (h). The corresponding hydrogen bonding network and density profiles were produced using the same approach as for the basal–basal interaction shown in Figure 4. Tilted side view in (a) shows nearly collapsing scenarios with sparse molecules on edges.

Therefore, the hydrogen bonding network is missing for (a). The figure and the axes in the last grid aid in orienting the edge–edge interface.

Similar to pure water, the energy barriers for edge-edge aggregation in the presence of pre-sorbed $NaNO_3$(aq) and KNO_3(aq) (Table 1 and Figures 3d, 3f) are also higher than those for basal-basal interactions. The barrier height for $NaNO_3$ (4.9 kJ/mol/nm^2) is smaller than that for KNO_3 (6.9 kJ/mol/nm^2), which suggests that $NaNO_3$ should generate a higher fraction of edge–edge aggregates than KNO_3. However, both are still large relative to that for basal–basal aggregation (~1 kJ/mol/nm^2). Figure 7 shows the structures of local minima of edge–edge aggregation for both $NaNO_3$(aq) and KNO_3(aq). In the presence of adsorbed ions, water density in the interlayer during aggregation is lower than in pure water, but still higher than in the basal–basal orientation (e.g., Figure 7d). The electrolyte densities at the interface (~0.01–0.04 number/Å^3, Figure 7d) are also higher than those for the basal–basal orientation at a similar interfacial distance (~ 0.01 number/Å^3, Figure 5c). The water density profile is also not symmetrical between the two interfaces as more cations occupy one side of the interface. This is due to the random initial distribution of ions in the interlayer and their small number, which leads to poor statistical sampling. Therefore, the higher energy barrier in the presence of electrolytes for edge–edge aggregation is likely due to the larger number of bonds, as with pure water.

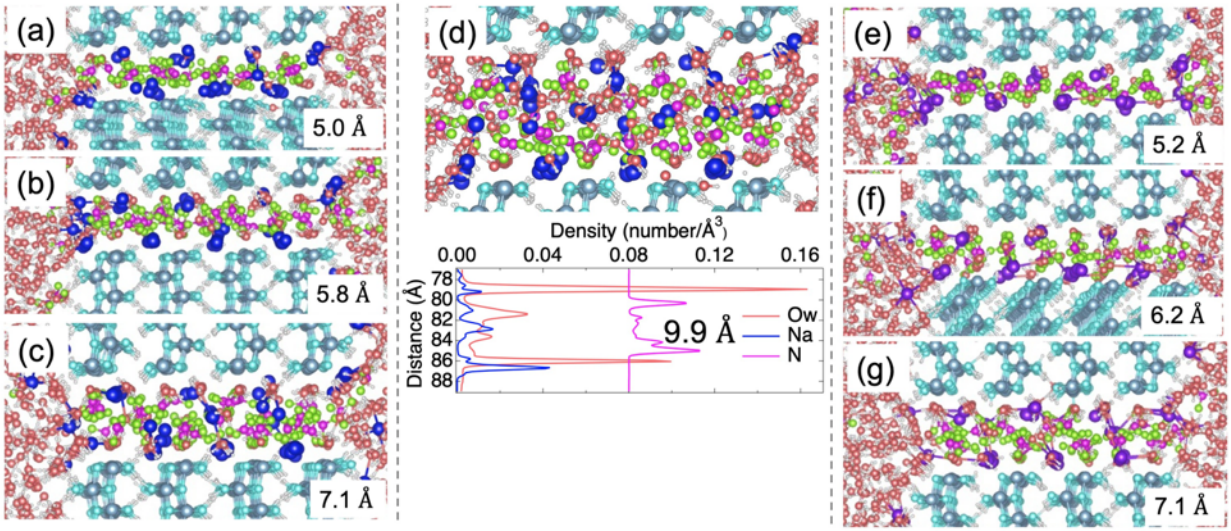

Figure 7. Local minima for boehmite particle aggregation in $NaNO_3$(aq) and KNO_3(aq). (a) – (d) are the local minima of $NaNO_3$(aq) in the interlayer at ~ 5 Å, ~ 5.8 Å, ~ 7.1 Å, and ~ 9.9 Å (with corresponding density profiles. The density of NO_3^- is offset by 0.08 unit for clarity), respectively. (e) – (g) are the local minima of KNO_3(aq) in the interlayer at ~ 5.2 Å, ~ 6.2 Å, and ~ 7.1 Å, respectively. These interfacial distances correspond to the local minima in Figures 3d, 3f. Lines between cations and Ow atoms indicate hydration bonding between cations and water molecules.

3.2 Cation and Surface Charge Effects

One challenge is to reconcile these results with prior measurements of aggregation, especially in the presence of different solute species and charged mineral surfaces. The interaction of the surface force apparatus was measured by Pashley[37] on mica and found the repulsive hydration force for monovalent cations $Li^+ \sim Na^+ > K^+ > Cs^+$. Multi-valent cations were also considered and have a larger interaction force, consistent with their increased propensity for adsorption[37,38]. In that study, the relative effects of sodium and potassium are the reverse of what is observed during aggregation of boehmite by Anovitz et al.[3], but the other ions are consistent where a large repulsive force corresponds to less extent of aggregation. During smectite clay particle aggregation by Shen et al., the relative repulsive forces were also measured $Na^+ > K^+$.[4] While the magnitudes of the repulsive forces in the current work are not precise here, the energy

barrier to aggregation for potassium is smaller than sodium, but sodium contains a deeper free energy minimum at a shorter distance (7.8-8.3 Å) (Figure S9 in the Supporting Information directly compares sodium and potassium free energy surfaces). If the comparison in Figure S9 below 7.8 Å is correct, this may indicate that sodium presents a larger repulsive force to aggregation, but a more stable state once the particles do become aggregated.

One important question is what we expect to happen if divalent (or trivalent) cations were instead present in this system. Since our results suggest that adsorption affinity is the most important driving factor for determining the magnitude of the effect the ion has on disrupting the interstitial solvation structure, we predict that higher valency ions will lead to a larger disruption of the interstitial solvent and hence, a larger reduction on the barriers to aggregation. Unfortunately, these simulations are sufficiently computationally demanding that an exhaustive probe of different possibilities is beyond the scope if this article, but certainly of interest in future work.

A further issue will be the effects of surface charge. As described in the Methods section above, the particles in this study are set to stoichiometric terminations with no surface charge. The experimental observation we are focusing on was performed where the solid was the only buffer of pH, and the pH migrated to pH 8-9, close to some literature values for the p.z.c. for boehmite platelets, 8.5[23]-9.5.[24,34] This corresponds to the p.z.c. of the basal (010) surface.[33] When surface charge is present, boehmite still has been observed to aggregate, e.g., at pH 11 (no added electrolyte, liquid-cell TEM)[33] and 12 (with added electrolyte, particle size by dynamic light scattering).[31] However, aggregation mechanism changes at higher pH, where an edge–edge aggregation is observed at higher pHs and basal–basal aggregation close to the p.z.c. as is simulated here.[33] Similar pH-dependent aggregation mechanisms have been observed on

558 serpentine ($Mg_3(Si_2O_5)(OH)_4$) where MgOH-SiO basal aggregation occurs at pH 5; while at pH 7
559 and 9, edge contacts also happen.[67] Thus, crystal-face specific aggregation is highly dependent on
560 the magnitude of the surface charge on different facets, but the current study demonstrates that
561 oriented attachment can also be driven without surface charge present.

562 More generally, we can expect two specific contributions of surface charge to the
563 aggregation extent. First, the long-range coulombic interaction of two mineral surfaces with charge
564 will lead to repulsion of the minerals. We speculate that since this interaction occurs at a longer
565 range nature (e.g., nanometers) than the forces observed here, a strongly repulsive coulombic
566 inhibit aggregation. A second, and more subtle effect, could be charge compensation. As stated
567 above, charge reversals at high solute concentration have sometimes been observed.[25] These are
568 interpreted as sufficient counterions adsorbing in a Stern layer to counteract, or even reverse, the
569 surface charge. Here, such a large number of adsorbed ions are predicted to significantly disrupt
570 the hydration structure, changing the energetics for aggregation, while also significantly reducing
571 the coulombic repulsion between particles.

572

573 ## 3.3 A Molecular Basis for Aggregation

574 When considered from a classical perspective such as DLVO theory,[6,7] the promotion of
575 aggregation by increasing ionic strength is interpreted as due to electrostatic screening of surface
576 charge by adsorbed ions and counterions in the diffuse layer, allowing dispersion or van der Waals
577 attractions to take over for aggregation of particles. It follows that oriented aggregation occurs
578 because different crystallographic surfaces have different surface charge densities.[33] As mentioned
579 above, however, the systems considered in the present study are stoichiometric, with no surface
580 charge. Thus, the origin of the differences in the energy barriers to aggregation observed here must

lie in the properties of the mineral-water interfaces themselves. Specifically, the extent of solvent ordering is likely a key parameter stabilizing a given hydration state during aggregation and creating energy barriers for the system to move between different aggregated states.

To test this hypothesis, we used unbiased simulations to calculate the water and ion peak and average densities at the distances of the energy minima and maxima (Figures 3 and 5). A selection of results is shown in Figure 8 (details are in Table S3 and Figures S10, S11 in the Supporting Information). Figures 8a and 8b display the results for pure water at the basal–basal interface, and Figures 8c and 8d display the results for water with electrolytes solution. Two measures were taken to compare the states between the energy minima and maxima: the highest or peak density of the water layer closest to the solid surface (Figures 8a, 8c, 8d), and the average number density of water in the entire interfacial region (Figure 8b). Peak density data were retrieved from Figures 4, and S6, S7 in the Supporting Information. The averaged values from two highest densities for the systems with electrolytes shown in Figures S6, S7 were used.

The peak densities of H_2O molecules show the same trend in pure water and electrolyte solutions, i.e., number density values at the energy minima are always higher than at the neighboring maxima. This indicates the closest interfacial layer always shows stronger water ordering at the energy minima states. Thus, the extent of water ordering that is likely the key to determining stable states, and the energy barriers to aggregation/disaggregation therefore stem from the energy required to disrupt the ordered water network. There are some exceptions, however. The first maxima at the lowest hydration states have a relatively high peak density and low average density (Figures 8a-d), and the value for the maximum at ~13 Å for $NaNO_3$ (Figure 8c) lies slightly above, rather than below the trend for the minima. This latter corresponds to a region between 12 and 13Å (Figure 3) in which the maxima and minima are poorly defined. Since

604 the peak densities in Figures 8c, 8d are lower than that in Figure 8a, it is assumed that the adsorbed
605 interfacial ions lower the energy barriers by disrupting the water hydrogen bonding network in the
606 interfacial layers.

607 Interestingly, the averaged densities for pure water at the energy maxima (Figure 8b) are
608 greater than for the minima states and become close to the value of bulk water (~0.033/Å^3) as the
609 distance increases. This is only explainable by suggesting that at an ordered mineral surface site-
610 water configuration (i.e., the minima), the need for a commensurate surface sites density and
611 sorbed water bonding network creates a lower density of water than is present in bulk water. When
612 this commensurate bonding environment is disrupted at the maxima, the water may take on a more
613 bulk-like configuration.

614 From another empirical point of view, the Hofmeister series[68] that describes the salt effects
615 for protein precipitation could be another test of the concepts in this manuscript. There is no
616 consensus on Na^+ and K^+ regarding their structure making/breaking capability ranking, however.
617 For example, Marcus[68] states the effects of Na^+ and K^+ are equivalent. Therefore, the simulation
618 results in this study and the empirical Hofmeister series are seemingly consistent. However, since
619 the crystal-face specific effects are observed here for the same ions, the Hofmeister series alone
620 cannot explain the results. In contrast, during flotation of soluble salts, Hancer et al.[69] and Du et
621 al.[70] find sodium acts as a structure maker and potassium as a structure breaker during flotation of
622 soluble salts. Part of the reason of the contradictory findings might be that there are system-specific
623 effects of given ions on aggregation, where different ions may have synergies or conflicts with
624 different mineral surfaces that promote different behaviors. In the future however, applied to a
625 broader series of ions, our findings may potentially be applied to aggregation more generally, e.g.,
626 for biomacromolecule assemblies.

Overall, these results are consistent with the idea that the synergy between the hydrogen-bonding network of interstitial water and the mineral surface sites determines both the extent of aggregation and the energetic barriers to it in this system. Furthermore, adsorbed ions can act to lower the energy barriers to aggregation by disrupting the hydrogen-bonded water networks during aggregation and allowing for a more flexible interstitial environment. This effect is independent of any effects of ions in the diffuse layer). As mentioned above, we believe ion specific effects observed previously[3] likely stem from the adsorption affinity of those ions, driven by a balance of different hydration free energy, size and charge of the ion, which in turn creates a variable magnitude of the effects observed here, i.e., the extent of water network ordering.

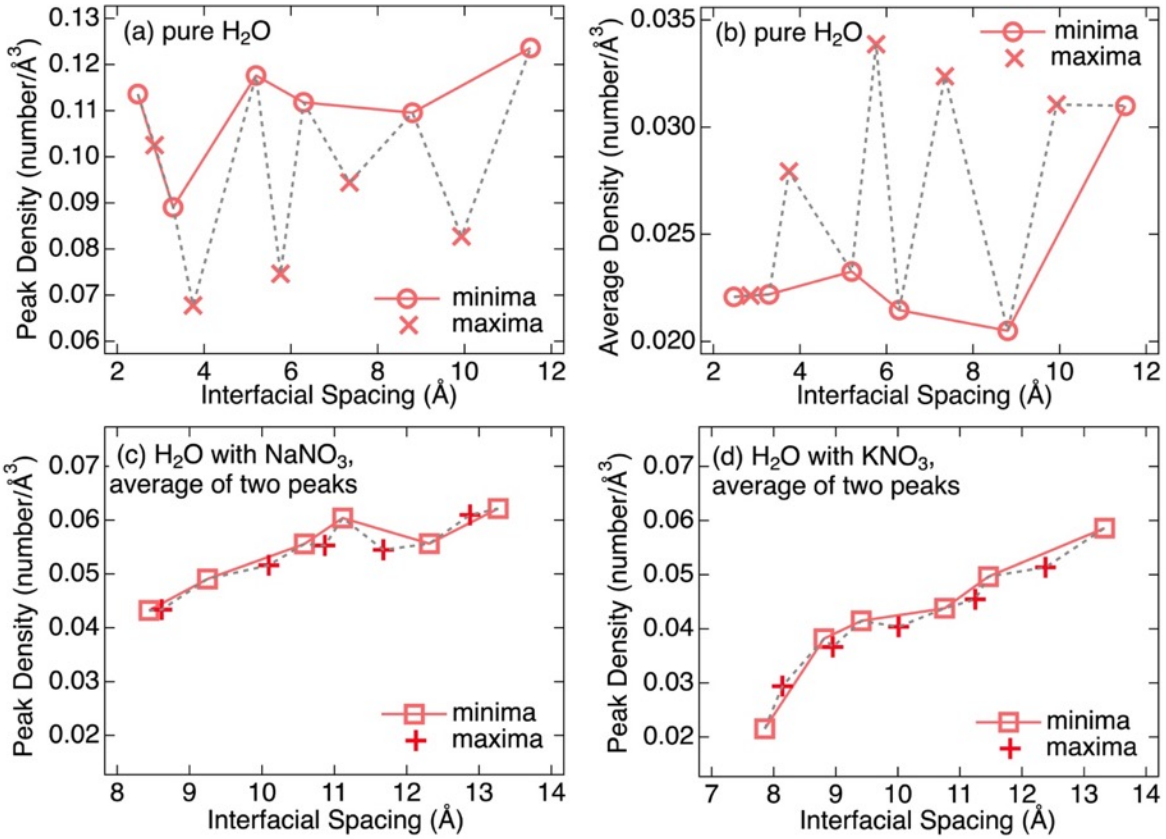

Figure 8. Peak densities of interfacial water molecules in the media of (a) pure water, (c) $NaNO_3$, and (d) KNO_3 for each minima and maxima of basal–basal aggregation. Average water density in the interface in the medium of pure water is shown in (b) for comparison.

5. Conclusions

This study was motivated by the experimental observation that the presence of alkali nitrates enhances boehmite nanoparticle aggregation, and the related more fundamental uncertainty as to what controls short-range forces driving aggregation at small distances. The metadynamics rare event theory simulations presented here allowed us to probe the energy barriers to aggregation with and without pre-sorbed electrolyte ions in the interlayer, as well as how these barriers differed between two crystal faces: basal–basal (010), and edge–edge (001). We found that the presence of $NaNO_3$ and KNO_3 lowered barriers to aggregation, and that basal–basal interactions were preferred over edge–edge interactions. Due to the smaller energy barriers, aggregates containing adsorbed ions in the interlayer are predicted to undergo more reversible aggregation/disaggregation. While the observations in this study are consistent with experimental work, there are a number of predictions that will need to be confirmed by experiments: first, we propose that both stable states and the magnitudes of the energy barriers between them stem from the relative ordering of the interstitial water network at mineral-surface sites. That is, energy minima occur where the mineral surface sites are commensurate with the hydrogen bonding environment for water monolayers, and energy barriers to aggregation derive from the need to perturb that ordered structure. Adsorbed ions promote aggregation by disrupting that interstitial water network, creating a more flexible environment for different aggregation states. Ion-specific effects are thus thought to derive from the differing ion concentrations in the interlayer. With this detailed interfacial structure and energetics information, further studies that couple the molecular-scale results on short-range interactions here with classical "dispersion forces" to predict particle aggregation across a range of solution compositions would be beneficial.

Supporting Information

Calculated hydration energy compared with empirical values; force field used in this study; estimation of the amount of adsorbed ions using adsorption free energy surface; aggregation in 0.1 m homogeneous electrolyte solutions; system converging with time; partial collapsing during basal–basal aggregation; additional two energy maximum states; structure comparison between local minimum and energy maximum states; interfacial water density profiles in presence of $NaNO_3$; interfacial water density profiles in presence of KNO_3; snapshots of the local minima of edge–edge aggregation; comparison of the repulsive hydration forces caused by $NaNO_3$ and KNO_3 in basal–basal aggregation; statistics of the numbers of species in the interfacial region and the corresponding number densities; plots of the number and number densities of the interfacial species as a function of interfacial spacing.

Declaration of competing interest

Authors declare no competing interests from this work.

Acknowledgements

This research was supported by Interfacial Dynamics in Radioactive Environments and Materials (IDREAM), an Energy Frontier Research Center funded by the U.S. Department of Energy (DOE), Office of Science, Basic Energy Sciences (BES) (FWP 68932). This research used resources of the National Energy Research Scientific Computing Center (NERSC), a U.S. Department of Energy Office of Science User Facility located at Lawrence Berkeley National Laboratory, operated under Contract No. DE-AC02-05CH11231.

References

(1) De Yoreo, J. J.; Gilbert, P. U. P. A.; Sommerdijk, N. A. J. M.; Penn, R. L.; Whitelam, S.; Joester, D.; Zhang, H.; Rimer, J. D.; Navrotsky, A.; Banfield, J. F.; Wallace, A. F.; Michel, F. M.; Meldrum, F. C.; Cölfen, H.; Dove, P. M. Crystallization by Particle Attachment in Synthetic, Biogenic, and Geologic Environments. *Science (1979)* **2015**, *349*, aaa6760. https://doi.org/10.1126/science.aaa6760.

(2) Hotze, E. M.; Phenrat, T.; Lowry, G. V. Nanoparticle Aggregation: Challenges to Understanding Transport and Reactivity in the Environment. *J Environ Qual* **2010**, *39*, 1909–1924. https://doi.org/10.2134/jeq2009.0462.

(3) Anovitz, L. M.; Huestis, P.; Rampal, N.; Stack, A. G.; LaVerne, J. A.; Zhang, X.; Schenter, G. K.; Chun, J.; Legg, B. A.; Liu, L.; Bleuel, M.; Gagnon, C.; Mildner, D. F. R. Frustrated Coulombic and Cation Size Effects on Nanoscale Boehmite Aggregation: A Tumbler Small- and Ultra-Small-Angle Neutron Scattering Study. *Journal of Physical Chemistry C* **2022**, *126*, 4391–4414. https://doi.org/10.1021/acs.jpcc.1c10580.

(4) Shen, X.; Bourg, I. C. Interaction between Hydrated Smectite Clay Particles as a Function of Salinity (0–1 M) and Counterion Type (Na, K, Ca). *Journal of Physical Chemistry C* **2022**, *126*, 20990–20997. https://doi.org/10.1021/acs.jpcc.2c04636.

(5) Shen, X.; Bourg, I. C. Molecular Dynamics Simulations of the Colloidal Interaction between Smectite Clay Nanoparticles in Liquid Water. *J Colloid Interface Sci* **2021**, *584*, 610–621. https://doi.org/10.1016/j.jcis.2020.10.029.

(6) Derjaguin, B. V.; Landau, L. D. Theory of the Stability of Strongly Charged Lyophobic Sols and of the Adhesion of Strongly Charged Particles in Solution of Electrolytes. *Acta Physicochim URSS* **1941**, *14*, 633.

(7) Vervey, E. J. W.; Overbeek, J. T. G.; van Nes, K. *Theory of Stability of Lyophobic Colloids: The Interaction of Sol Particles Having an Electric Double Layer.*; Elsevier: Amsterdam, 1948.

(8) Israelachvili, J. N. *Intermolecular and Surface Forces*; Academic Press: Waltham, MA, 2011.

(9) Nakouzi, E.; Kerisit, S.; Legg, B. A.; Yadav, S.; Li, D.; Stack, A. G.; Mundy, C. J.; Chun, J.; Schenter, G. K.; De Yoreo, J. J. Solution Structure and Hydration Forces between Mica and Hydrophilic Versus Hydrophobic Surfaces. *Journal of Physical Chemistry C* **2023**, *127*, 2741–2752. https://doi.org/10.1021/acs.jpcc.2c09120.

(10) Israelachvili, J. N.; Pashley, R. M. Molecular Layering of Water at Surfaces and Origin of Repulsive Hydration Forces. *Nature* **1983**, *306*, 249–250.

(11) Espinosa-Marzal, R. M.; Drobek, T.; Balmer, T.; Heuberger, M. P. Hydrated-Ion Ordering in Electrical Double Layers. *Physical Chemistry Chemical Physics* **2012**, *14*, 6085–6093. https://doi.org/10.1039/c2cp40255f.
(12) Ho, T. A.; Criscenti, L. J. Molecular-Level Understanding of Gibbsite Particle Aggregation in Water. *J Colloid Interface Sci* **2021**, *600*, 310–317. https://doi.org/10.1016/j.jcis.2021.05.016.
(13) Ho, T. A.; Rosso, K. M.; Criscenti, L. J. Atomistic Mismatch Defines Energy–Structure Relationships during Oriented Attachment of Nanoparticles. *Journal of Physical Chemistry Letters* **2022**, *13*, 9339–9347. https://doi.org/10.1021/acs.jpclett.2c02511.
(14) Iijima, S.; Yumura, T.; Liu, Z. One-Dimensional Nanowires of Pseudoboehmite (Aluminum Oxyhydroxide γ-AlOOH). *Proc Natl Acad Sci U S A* **2016**, *113*, 11759–11764. https://doi.org/10.1073/pnas.1614059113.
(15) Nakouzi, E.; Stack, A. G.; Kerisit, S.; Legg, B. A.; Mundy, C. J.; Schenter, G. K.; Chun, J.; De Yoreo, J. J. Moving beyond the Solvent-Tip Approximation to Determine Site-Specific Variations of Interfacial Water Structure through 3D Force Microscopy. *Journal of Physical Chemistry C* **2021**, *125*, 1282–1291. https://doi.org/10.1021/acs.jpcc.0c07901.
(16) Peterson, R. A.; Buck, E. C.; Chun, J.; Daniel, R. C.; Herting, D. L.; Ilton, E. S.; Lumetta, G. J.; Clark, S. B. Review of the Scientific Understanding of Radioactive Waste at the U.S. DOE Hanford Site. *Environ Sci Technol* **2018**, *52*, 381–396. https://doi.org/10.1021/acs.est.7b04077.
(17) Wells, B. E.; Onishi, Y.; Burns, C. A.; Daniel, R. C.; Kurath, D. E.; Huckaby, J. L.; Buck, E. C.; Anderson, K. K.; Mahoney, L. A.; Cooley, S. K.; Tingey, J. M. *Hanford Waste Physical and Rheological Properties: Data and Gaps*; Richland, WA, 2011.
(18) Poloski, A. P.; Tingey, J. M.; Wells, B. E.; Mahoney, L. A.; Hall, M. N.; Smith, G. L.; Thomson, S. L.; Johnson, M. E.; Knight, M. A.; Meacham, J. E.; Thien, M. J.; Davis, H. J. J.; Onishi, Y. *Estimate of Hanford Waste Rheology and Settling Behavior*; Richland, WA, 2007.
(19) Golcar, G. R.; Colton, N. G.; Darab, J. G.; Smith, H. D. *Hanford Tank Waste Simulants Specification and Their Applicability for the Retrieval, Pretreatment, and Vitrification Processes*; Richland, Washington, 2000.
(20) US DOE. *2019 Hanford Lifecycle Scope, Schedule and Cost Report*; Richland Operations Office.
(21) *Basic Research Needs for Environmental Management Report of the Office of Science Workshop on Environmental Management*; 2016. http://science.energy.gov/~/media/bes/pdf/reports/files/BRNEM_rpt.pdf.
(22) Page, J. S.; Reynolds, J. G.; Cooke, G. A.; Wells, B. E. Large Cemented Gibbsite Agglomerates in Alkaline Nuclear Waste at the Hanford Site and the Impacts to Remediation. *J Hazard Mater* **2020**, *384*, 121318. https://doi.org/10.1016/j.jhazmat.2019.121318.
(23) Wood, R.; Fornasiero, D.; Ralston, J. Electrochemistry of the Boehmite—Water Interface. *Colloids and surfaces* **1990**, *51*, 389–403.
(24) Smith, W.; Pouvreau, M.; Rosso, K.; Clark, A. E. PH Dependent Reactivity of Boehmite Surfaces from First Principles Molecular Dynamics. *Physical Chemistry Chemical Physics* **2022**, *24*, 14177–14186. https://doi.org/10.1039/d2cp00534d.

(25) Hakim, A.; Nishiya, M.; Kobayashi, M. Charge Reversal of Sulfate Latex Induced by Hydrophobic Counterion: Effects of Surface Charge Density. *Colloid Polym Sci* **2016**, *294*, 1671–1678. https://doi.org/10.1007/s00396-016-3931-6.
(26) Wesolowski, D. J.; Ziemniak, S. E.; Anovitz, L. M.; Machesky, M. L.; Bénézeth, P.; Palmer, D. A. Solubility and Surface Adsorption Characteristics of Metal Oxides. In *Aqueous Systems at Elevated Temperatures and Pressures: Physical Chemistry in Water, Steam and Hydrothermal Solutions*; Palmer, D. A., Fernández-Prini, R., Harvey, A. H., Eds.; Academic Press, 2004; pp 493–595.
(27) Furusawa, K.; Kakoki, H.; Matsumura, H. Colloid Chemical Studies on the Aggregation of Phospholipid Vesicles with Metal Cations. *Bull. Chem. Soc. Jpn.* **1984**, *57*, 3413–3418.
(28) Wang, H.; Zhao, X.; Han, X.; Tang, Z.; Liu, S.; Guo, W.; Deng, C.; Guo, Q.; Wang, H.; Wu, F.; Meng, X.; Giesy, J. P. Effects of Monovalent and Divalent Metal Cations on the Aggregation and Suspension of Fe3O4 Magnetic Nanoparticles in Aqueous Solution. *Science of the Total Environment* **2017**, *586*, 817–826. https://doi.org/10.1016/j.scitotenv.2017.02.060.
(29) Pavlovic, M.; Rouster, P.; Oncsik, T.; Szilagyi, I. Tuning Colloidal Stability of Layered Double Hydroxides: From Monovalent Ions to Polyelectrolytes. *Chempluschem* **2017**, *82*, 121–131. https://doi.org/10.1002/cplu.v82.1.
(30) Li, D.; Chen, Q.; Chun, J.; Fichthorn, K.; De Yoreo, J.; Zheng, H. Nanoparticle Assembly and Oriented Attachment: Correlating Controlling Factors to the Resulting Structures. *Chemical Reviews*. American Chemical Society March 22, 2023, pp 3127–3159. https://doi.org/10.1021/acs.chemrev.2c00700.
(31) Anovitz, L. M.; Zhang, X.; Soltis, J.; Nakouzi, E.; Krzysko, A. J.; Chun, J.; Schenter, G. K.; Graham, T. R.; Rosso, K. M.; De Yoreo, J. J.; Stack, A. G.; Bleuel, M.; Gagnon, C.; Mildner, D. F. R.; Ilavsky, J.; Kuzmenko, I. Effects of Ionic Strength, Salt, and PH on Aggregation of Boehmite Nanocrystals: Tumbler Small-Angle Neutron and X-Ray Scattering and Imaging Analysis. *Langmuir* **2018**, *34*, 15839–15853. https://doi.org/10.1021/acs.langmuir.8b00865.
(32) Nakouzi, E.; Soltis, J. A.; Legg, B. A.; Schenter, G. K.; Zhang, X.; Graham, T. R.; Rosso, K. M.; Anovitz, L. M.; De Yoreo, J. J.; Chun, J. Impact of Solution Chemistry and Particle Anisotropy on the Collective Dynamics of Oriented Aggregation. *ACS Nano* **2018**, *12*, 10114–10122. https://doi.org/10.1021/acsnano.8b04909.
(33) Liu, L.; Legg, B. A.; Smith, W.; Anovitz, L. M.; Zhang, X.; Harper, R.; Pearce, C. I.; Rosso, K. M.; Stack, A. G.; Bleuel, M.; Mildner, D. F. R.; Schenter, G. K.; Clark, A. E.; De Yoreo, J. J.; Chun, J.; Nakouzi, E. Predicting Outcomes of Nanoparticle Attachment by Connecting Atomistic, Interfacial, Particle, and Aggregate Scales. *ACS Nano* **2023**, *17*, 15556–15567. https://doi.org/10.1021/acsnano.3c02145.
(34) Alwitt, R. S. The Point of Zero Charge of Pseudoboehmite. *J Colloid Interface Sci* **1972**, *40*, 195–198.
(35) Kaledin, L. A.; Tepper, F.; Kaledin, T. G. Pristine Point of Zero Charge (p.p.z.c.) and Zeta Potentials of Boehmites Nanolayer and Nanofiber Surfaces. *Int J Smart Nano Mater* **2016**, *7*, 1–21. https://doi.org/10.1080/19475411.2016.1148077.
(36) Pashley, R. M. Hydration Forces between Mica Surfaces in Electrolyte Solutions. *Adv Colloid Interface Sci* **1982**, *16*, 57–62.

(37) Pashley, R. M.; Quirk, J. P. The Effect of Cation Valency on DLVO and Hydration Forces between Macroscopic Sheets of Muscovite Mica in Relation to Clay Swelling. *Colloids and Surfaces* **1984**, *9*, 1–17.
(38) Pashley, R. M.; Israelachvili, J. N. DLVO and Hydration Forces between Mica Surfaces in Mg2+, Ca2+, Sr2+, and Ba2+ Chloride Solutions. *J Colloid Interface Sci* **1984**, *97*, 446–455.
(39) Pashley, R. M. DLVO and Hydration Forces between Mica Surfaces in Li+, Na+, K+, and Cs+ Electrolyte Solutions: A Correlation of Double-Layer and Hydration Forces with Surface Cation Exchange Properties. *J Colloid Interface Sci* **1981**, *83*, 531–546.
(40) Diao, Y.; Han, M.; Lopez-Berganza, J. A.; Valentino, L.; Marinas, B.; Espinosa-Marzal, R. M. Reconciling DLVO and Non-DLVO Forces and Their Implications for Ion Rejection by a Polyamide Membrane. *Langmuir* **2017**, *33*, 8982–8992. https://doi.org/10.1021/acs.langmuir.7b02306.
(41) Ilgen, A. G.; Leung, K.; Criscenti, L. J.; Greathouse, J. A. Adsorption at Nanoconfined Solid-Water Interfaces. *Annu Rev Phys Chem* **2023**, *74*, 169–191. https://doi.org/10.1146/annurev-physchem-083022.
(42) Acuña, S. M.; Toledo, P. G. Nanoscale Repulsive Forces between Mica and Silica Surfaces in Aqueous Solutions. *J Colloid Interface Sci* **2011**, *361*, 397–399. https://doi.org/10.1016/j.jcis.2011.05.063.
(43) Thompson, A. P.; Aktulga, H. M.; Berger, R.; Bolintineanu, D. S.; Brown, W. M.; Crozier, P. S.; in 't Veld, P. J.; Kohlmeyer, A.; Moore, S. G.; Nguyen, T. D.; Shan, R.; Stevens, M. J.; Tranchida, J.; Trott, C.; Plimpton, S. J. LAMMPS - a Flexible Simulation Tool for Particle-Based Materials Modeling at the Atomic, Meso, and Continuum Scales. *Comput Phys Commun* **2022**, *271*, 108171. https://doi.org/10.1016/j.cpc.2021.108171.
(44) Brown, W. M.; Kohlmeyer, A.; Plimpton, S. J.; Tharrington, A. N. Implementing Molecular Dynamics on Hybrid High Performance Computers – Particle–Particle Particle–Mesh. *Comput Phys Commun* **2012**, *183*, 449–459. https://doi.org/10.1016/j.cpc.2011.10.012.
(45) Cygan, R. T.; Liang, J.-J.; Kalinichev, A. G. Molecular Models of Hydroxide, Oxyhydroxide, and Clay Phases and the Development of a General Force Field. *Journal of Physical Chemistry B* **2004**, *108*, 1255–1266. https://doi.org/10.1021/jp0363287.
(46) Cygan, R. T.; Greathouse, J. A.; Kalinichev, A. G. Advances in Clayff Molecular Simulation of Layered and Nanoporous Materials and Their Aqueous Interfaces. *Journal of Physical Chemistry C* **2021**, *125*, 17573–17589. https://doi.org/10.1021/acs.jpcc.1c04600.
(47) Greathouse, J. A.; Durkin, J. S.; Larentzos, J. P.; Cygan, R. T. Implementation of a Morse Potential to Model Hydroxyl Behavior in Phyllosilicates. *J Chem Phys* **2009**, *130*, 134713. https://doi.org/10.1063/1.3103886.
(48) Pouvreau, M.; Greathouse, J. A.; Cygan, R. T.; Kalinichev, A. G. Structure of Hydrated Kaolinite Edge Surfaces: DFT Results and Further Development of the ClayFF Classical Force Field with Metal-O-H Angle Bending Terms. *Journal of Physical Chemistry C* **2019**, *123*, 11628–11638. https://doi.org/10.1021/acs.jpcc.9b00514.
(49) Pouvreau, M.; Greathouse, J. A.; Cygan, R. T.; Kalinichev, A. G. Structure of Hydrated Gibbsite and Brucite Edge Surfaces: DFT Results and Further Development of the ClayFF Classical Force Field with Metal-O-H Angle Bending Terms. *Journal of Physical Chemistry C* **2017**, *121*, 14757–14771. https://doi.org/10.1021/acs.jpcc.7b05362.

(50) Berendsen, H. J. C.; Grigera, J. R.; Straatsma, T. P. The Missing Term in Effective Pair Potentials. *J. Phys. Chem.* **1987**, *91* (24), 6269–6271.
(51) Christensen, A. N.; Lehmann, M. S.; Convert, P. Deuteration of Crystalline Hydroxides. Hydrogen Bonds of γ-AlOO(H,D) and γ-FeOO(H,D). *Acta Chemica Scandinavica A* **1982**, *36*, 303–308.
(52) Stack, A. G. Molecular Dynamics Simulations of Solvation and Kink Site Formation at the {001} Barite-Water Interface. *Journal of Physical Chemistry C* **2009**, *113*, 2104–2110. https://doi.org/10.1021/jp8062993.
(53) Fantauzzo, V.; Yeandel, S. R.; Freeman, C. L.; Harding, J. H. A Transferable Force-Field for Alkali Metal Nitrates. *J Phys Commun* **2022**, *6*, 055011. https://doi.org/10.1088/2399-6528/ac6e2b.
(54) Wang, H.-W.; Vlcek, L.; Neuefeind, J. C.; Page, K.; Irle, S.; Simonson, J. M.; Stack, A. G. Decoding Oxyanion Aqueous Solvation Structure: A Potassium Nitrate Example at Saturation. *Journal of Physical Chemistry B* **2018**, *122*, 7584–7589. https://doi.org/10.1021/acs.jpcb.8b05895.
(55) Megyes, T.; Bálint, S.; Peter, E.; Grósz, T.; Bakó, I.; Krienke, H.; Bellissent-Funel, M. C. Solution Structure of NaNO3 in Water: Diffraction and Molecular Dynamics Simulation Study. *Journal of Physical Chemistry B* **2009**, *113*, 4054–4064. https://doi.org/10.1021/jp806411c.
(56) Pérez-Sánchez, G.; Galvão, T. L. P.; Tedim, J.; Gomes, J. R. B. A Molecular Dynamics Framework to Explore the Structure and Dynamics of Layered Double Hydroxides. *Appl Clay Sci* **2018**, *163*, 164–177. https://doi.org/10.1016/j.clay.2018.06.037.
(57) Cadena, C.; Maginn, E. J. Molecular Simulation Study of Some Thermophysical and Transport Properties of Triazolium-Based Ionic Liquids. *Journal of Physical Chemistry B* **2006**, *110*, 18026–18039. https://doi.org/10.1021/jp0629036.
(58) Stack, A. G.; Rustad, J. R. Structure and Dynamics of Water on Aqueous Barium Ion and the {001} Barite Surface. *Journal of Physical Chemistry C* **2007**, *111*, 16387–16391. https://doi.org/10.1021/jp0747196.
(59) Rampal, N.; Wang, H.-W.; Biriukov, D.; Brady, A. B.; Neuefeind, J. C.; Předota, M.; Stack, A. G. Local Molecular Environment Drives Speciation and Reactivity of Ion Complexes in Concentrated Salt Solution. *J Mol Liq* **2021**, *340*, 116898. https://doi.org/10.1016/j.molliq.2021.116898.
(60) Martínez, L.; Andrade, R.; Birgin, E. G.; Martínez, J. M. PACKMOL: A Package for Building Initial Configurations for Molecular Dynamics Simulations. *J Comput Chem* **2009**, *30*, 2157–2164. https://doi.org/10.1002/jcc.21224.
(61) The PLUMED consortium. Promoting Transparency and Reproducibility in Enhanced Molecular Simulations. *Nat Methods* **2019**, *16*, 667–673. https://doi.org/10.1038/s41592-019-0475-y.
(62) Bonomi, M.; Branduardi, D.; Bussi, G.; Camilloni, C.; Provasi, D.; Raiteri, P.; Donadio, D.; Marinelli, F.; Pietrucci, F.; Broglia, R. A.; Parrinello, M. PLUMED: A Portable Plugin for Free-Energy Calculations with Molecular Dynamics. *Comput Phys Commun* **2009**, *180*, 1961–1972. https://doi.org/10.1016/j.cpc.2009.05.011.
(63) Tribello, G. A.; Bonomi, M.; Branduardi, D.; Camilloni, C.; Bussi, G. PLUMED 2: New Feathers for an Old Bird. *Comput Phys Commun* **2014**, *185*, 604–613. https://doi.org/10.1016/j.cpc.2013.09.018.

(64) Raiteri, P.; Laio, A.; Gervasio, F. L.; Micheletti, C.; Parrinello, M. Efficient Reconstruction of Complex Free Energy Landscapes by Multiple Walkers Metadynamics. *Journal of Physical Chemistry B* **2006**, *110*, 3533–3539. https://doi.org/10.1021/jp054359r.

(65) Li, D.; Chun, J.; Xiao, D.; Zhou, W.; Cai, H.; Zhang, L.; Rosso, K. M.; Mundy, C. J.; Schenter, G. K.; De Yoreo, J. J. Trends in Mica–Mica Adhesion Reflect the Influence of Molecular Details on Long-Range Dispersion Forces Underlying Aggregation and Coalignment. *Proc Natl Acad Sci U S A* **2017**, *114*, 7537–7542. https://doi.org/10.1073/pnas.1621186114.

(66) Ho, T. A.; Criscenti, L. J.; Greathouse, J. A. Revealing Transition States during the Hydration of Clay Minerals. *Journal of Physical Chemistry Letters* **2019**, *10*, 3704–3709. https://doi.org/10.1021/acs.jpclett.9b01565.

(67) Wang, Z.; Xiang, Y.; Wang, D.; Xu, L.; Xing, Y.; Gao, Z.; Sun, W.; Xie, L. Facet-Dependent Charge Density of Serpentine: Nanoscopic Implications for Aggregation and Entrainment of Fine Particles. *Langmuir* **2023**, *39*, 19027–19036. https://doi.org/10.1021/acs.langmuir.3c03227.

(68) Marcus, Y. Effect of Ions on the Structure of Water: Structure Making and Breaking. *Chem Rev* **2009**, *109*, 1346–1370. https://doi.org/10.1021/cr8003828.

(69) Hancer, M.; Celik, M. S.; Miller, J. D. The Significance of Interfacial Water Structure in Soluble Salt Flotation Systems. *J Colloid Interface Sci* **2001**, *235*, 150–161. https://doi.org/10.1006/jcis.2000.7350.

(70) Du, H.; Ozdemir, O.; Wang, X.; Cheng, F.; Celik, M. S.; Miller, J. D. Flotation Chemistry of Soluble Salt Minerals: From Ion Hydration to Colloid Adsorption. *Minerals & Metallurgical Processing* **2014**, *31*, 1–20.